Both experimental and molecular dynamics approaches highlight the central role of interfacial water for radical production by irradiated gold nanoparticles

Emilie Brun, Rika Tandiana, Manon Gilles, Yannis Cheref, Nguyen-Thi Van-Oanh, Carine Clavaguera, Cécile Sicard-Roselli

Title

Both experimental and molecular dynamic approaches highlight the central role of interfacial water for radical production by irradiated gold nanoparticles

Authors

Emilie Brun[1], Rika Tandiana[1], Manon Gilles[1], Yannis Cheref [1,2*,3*], Nguyen-Thi Van-Oanh[1], Carine Clavaguera[1] and Cécile Sicard-Roselli[1]

[1] Université Paris-Saclay, CNRS, Institut de Chimie Physique UMR 8000, 91405, Orsay Cedex, France;

[2] Institut Lumière Matière, Université Claude Bernard Lyon 1, CNRS UMR 5306, Villeurbanne, F-69622, France.

[3] Laboratoire de Chimie Lyon, École Normale Supérieure de Lyon, Université Claude Bernard Lyon 1, CNRS UMR 5182,

Lyon, 69364, France.

* : present address

Keywords

Gold, metallic nanoparticles, radiation, radiosensitization, radicals, simulation.

Abstract

Nanoparticles devoted to improve radiotherapy treatments are an efficient tool if they can induce the formation of deleterious species in the tumor. Their interaction with radiation is responsible for radical production but in spite of the numerous studies mostly with cells, no consensus is reached about their formation mechanism. In order to gain in knowledge, we applied a very sensitive test to quantify hydroxyl radicals and electrons produced when gold atoms, organized as nanoparticles or as a salt in solution, are irradiated by keV and MeV photons (X- and γ- Rays). Crucial role of interfacial water is suggested to explain the high quantity of radicals measured for nanoparticles. These experimental data were supplemented by classical molecular dynamic simulation, revealing a specific organization of the water hydrogen bonding network at the nanoparticle surface which could be a key component in the mechanism of radical production by irradiated colloidal suspensions.

Introduction

Nanomedicine is one of the fastest growing areas in nanotechnology. In particular cancer nanotechnology is steadily progressing: as cancer statistics are only improving slowly, there is a need for new approaches. Liposomes, polymeric micelles, and nanoparticles (NPs) are the most studied nanostructures. Among them, manufactured gold nanoparticles (GNPs) have been constantly developed for biomedical applications, be it for diagnosis [1] or therapy [2]. The enthusiasm aroused by their unique properties, among which spectroscopic and catalytic, and the possible progress they could generate, lead some to talk about a new “Golden Age” [3]. Almost twenty years ago, Hainfeld was the first to use GNP to enhance radiotherapy in mice [4]. This pioneering work opened perspectives in the search of new

radiosensitizers/radioenhancers to achieve better treatment outcomes. Since then, studies on animals, cells and biomolecules have confirmed this effect with unexpected contradictory results [5-7]. Basically, last decades have been less successful than expected as regards clinical translation of GNP for radiosensitization. Among nanosized radiosensitizers, only two candidates are in clinical evaluation, namely AGuIX® (NH TherAguix, Lyon, France) and NBTXR3/Hensify® (Nanobiotix, Paris, France), based respectively on gadolinium and hafnium.

Given the wide panel of NP used, in terms of core nature, size, coating, not to mention of cell lines and irradiation modalities, cross-comparison of data is not a walk in the park. But this complexity also seems to arise from a fragmentary knowledge of the mechanisms at stage, which is another obstacle to the design of an efficient radiosensitizing NP. Indeed, the main rationale for developing metallic NP as dose enhancers, and the first explanation for their radiosensitizing capacities, when irradiated with low energy keV photons, is their higher mass energy absorption coefficient compared to water or soft tissues.

The first step of the interaction between GNPs and radiation relies on the physical dose which represents supplementary energy absorbed by nanomaterials followed by electron ejections (Auger and photoelectrons). According to Monte Carlo simulations, Auger electrons contribute to low-range (~10 nm) dose enhancement, while electrons of higher energy (photo- or Compton electrons) contribute to enhancement at a μm scale (up to 30–40 μm)[8]. These electrons are the main cause of a secondary physico-chemical step in which they should interact with surrounding water molecules leading to secondary radiolysis [9]. Among the main species produced are very reactive radicals: solvated electrons, hydroxyl radicals ($HO^{\bullet}$), hydrogen atoms ($H^{\bullet}$), and superoxide radical anions ($O_2^{\bullet -}$) in the presence of oxygen. These species are involved in the third step of the phenomenon which is their capacity to induce biological damages, often measured as clonogenic cell death in cellular experiments or DNA double strand

breaks foci. Through a precise analysis of the literature and focusing on quantitative aspects, we can wonder if there is a link between the dose enhancement calculated, the quantities of radicals formed and the relative biological effectiveness (RBE). Indeed, when irradiation is performed with MeV photons, physical dose enhancement was simulated to be negligible even for high-Z NPs [10], while *in vitro* and *in vivo* dose enhancement findings have been reported [11].

To address this question and in order to obtain a full description of the radiosensitization phenomenon, we developed a protocol to quantify hydroxyl radicals and solvated electrons in the presence of GNP [12]. In this work, we will present the experimental results obtained for GNP of 6 nm of diameter regarding the production of radicals under low and high energy photon irradiation, but also simulation results investigating water organization near the GNP surface.

Methods

Gold nanoparticle synthesis and characterization

Synthesis

Gold nanoparticles were prepared from $KAuCl_4$ salt. A 0.125 mM solution was reduced with tri-sodium citrate (0.04% $m.w^{-1}$ final concentration) and tannic acid (0.05% $m.w^{-1}$ final concentration) at 60 °C. In order to get rid of most of reactants, the obtained nanoparticle solution was washed at least three times by centrifugation at 190 000g for 30 minutes. At each step, the supernatant and the tannic acid pellet were withdrawn. Only the gold nanoparticle pellet was collected and resuspended in pure water.

Transmission Electron Microscopy (TEM)

Nanoparticles were observed on a JEOL JEM-1400 microscope operating at 120 kV. Images were acquired using a postcolumn high-resolution (11 megapixels) high-speed camera (SC1000 Orius, Gatan), then processed with Digital Micrograph (Gatan) and ImageJ software.

Concentration determination

To determine the nanoparticle concentration, an absorption spectrum was recorded on an Evolution 500 (Thermo Electron Corporation) spectrophotometer. Equation 1 was used to obtain the molar extinction coefficient (in $L.mol^{-1}.cm^{-1}$) from the volume (in nm^3) determined by TEM measurements.

$\log \varepsilon = 1.04 \log V + 5.18$ Eq.1

Irradiation modalities

X-Ray photons provided by an apparatus adapted from a Diffractis 583 X-ray generator (Enraf Nonius, Mo cathod) were non-monochromatic X-rays of 17.5 keV effective energy. Irradiations were performed at 20 $Gy.min^{-1}$ in a 0-15 Gy dose range.

Gamma ray photons (ca. 1.2 MeV) were produced with a panoramic gamma source (^{60}Co) (IL60PL Cis-Bio International).

Dose determination was performed with the Fricke dosimeter quantifying the oxidation of ferrous ions in ferric ions, considering $G(Fe^{3+}) = 1.42$ $\mu mol.J^{-1}$ at 17.5 keV and $G(Fe^{3+}) = 1.61$ $\mu mol.J^{-1}$ for γ-rays [13].

Radical quantification

Coumarin assay was used to measure the hydroxyl radical production. 7-hydroxycoumarin fluorescence quantification was performed on a Synergy H1 microplate reader (BioTek) at 25°C. Excitation wavelength was set at 326 nm and maximal emission intensity was quantified

at ca. 450 nm. Before fluorescence measurements, nanoparticles were removed from samples by adding a NaCl solution (1 % w/v final concentration) to induce particle aggregation followed by centrifugation to remove any gold aggregate from the solution (19 275 g, 10 min).

To quantify electrons, the same coumarin assay was employed but all samples were degassed at least one hour with N_2O before irradiation in order to transform electrons in hydroxyl radicals according to equation 2.

$$e^-_{solv.} + N_2O + H_2O \rightarrow HO^\bullet + HO^- + N_2 \qquad \text{Eq. 2}$$

Simulation

Classical molecular dynamics and quantum and semi-empirical methods were already described in Tandiana et al [14].

Results

In order to determine radicals produced when nanoparticles are irradiated, we decided to consider small gold nanoparticles (GNPs). The choice of gold among the different metallic nanoparticles has several motivations. Since the pioneering work of Hainfeld in 2004 [15], the radiosensitizing properties of GNP have been demonstrated under a wide variety of experimental conditions (size and coating of NPs, cell models, keV and MeV photons, heavy ions, …) [10-11, 16]. Most of the studies dealing with the physico-chemical mechanisms at stage are focused on GNP, using plasmid DNA or other radical probes as targets [6, 17], providing data in cell-free systems. GNP are also predominantly chosen as model nanoparticles

for Monte Carlo simulations[18-19]. Finally, contrary to other radiosensitizers such as AGuIX®, which is a nanosized platform gathering *ca* 15 individual gadolinium atoms, GNP are "real" nanoparticles in which collective effects can manifest. In this work, we decided to focus on ultrasmall (<10 nm) GNPs. Such NPs have been proved to be promising in biomedical applications, especially for cancer diagnosis and therapy as recently reviewed [20]. They present more effective renal clearance than their larger counterparts, minimizing any potential side effects related to gold accumulation. This is of utmost importance as, contrary to the accepted dogma of gold inertness, biotransformation of GNP was recently demonstrated in fibroblasts [21]. Ultrasmall GNPs show higher tumor tissue permeability and the smaller (2-6 nm) were shown once to be able to penetrate into the nucleus [22]. We also decided to investigate non-intentionally coated NPs as previous works from our group and others demonstrated that coating can decrease the quantity of radicals inducing cell component damages [23-25].

Whatever the nanoparticles considered, the first compulsory step is to obtain a very precise characterization of the nano-objects considering size, morphology and concentration. Hence, after synthesis, we first visualized the nanoparticles with electron microscopy (Figure 1). The representative transmission electron microscopy (TEM) image in Figure 1A shows that the prepared GNPs exhibit spherical morphology and display a narrow size distribution in the range 3-9 nm with a mean of 6.1 ± 0.8 nm. Each synthesis was controlled by TEM, to determine the mean diameter and infer the molar extinction coefficient of the plasmon band ($2.2\ 10^7$ $L.mol^{-1}.cm^{-1}$ for a 6.1 nm synthesis for example). This allows to control and verify the concentration of the suspension before irradiation experiment.

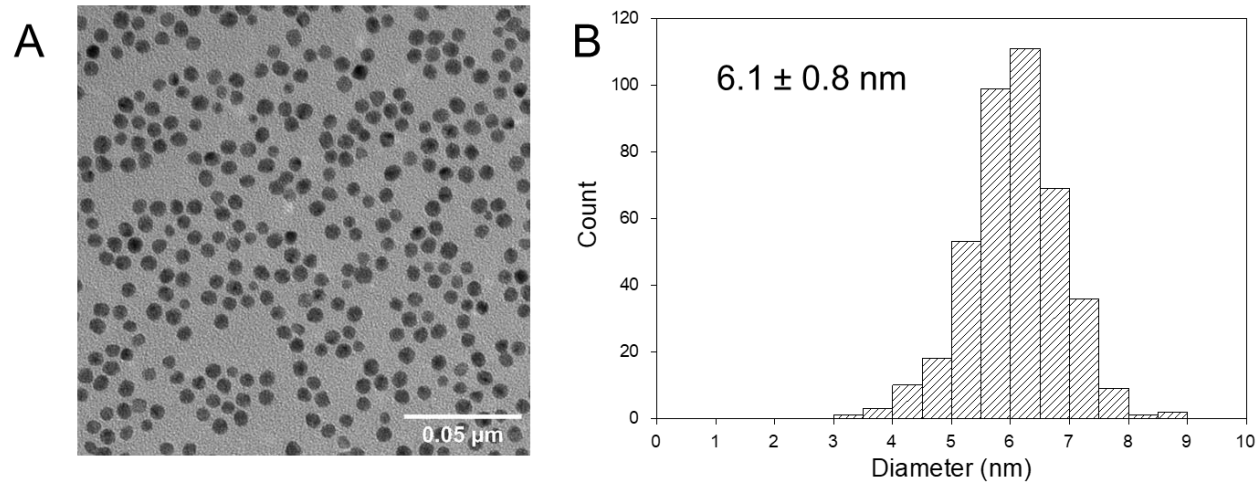

Figure 1 : A-Representative TEM image of the gold nanoparticles used in this study. B-Size distribution after diameter measurement of 412 objects. The mean and standard deviation of the population are indicated.

To quantify hydroxyl radicals *in vitro,* we adapted a protocol to make it compatible with the presence of nano-objects[12]. This protocol is based on the coumarin probe oxidation. Coumarin reacts with $HO^{\bullet}$ with a constant rate of $1{,}05.10^{10}$ $L.mol^{-1}.s^{-1}$ [26] to give several hydroxylation products among which 7-hydroxycoumarin (7-OH coumarin) is strongly fluorescent. In a typical experiment, nanoparticle solutions are irradiated in the presence of 0.5 mM of coumarin at different irradiation doses (0-15 Gy), GNP are removed and supernatant fluorescence spectrum are recorded. Plotted as a function of the dose, fluorescence intensity at 450 nm always presents a linear evolution, as can be seen on Figure 2A. A calibration curve allows to convert 7-OH coumarin fluorescence signal into concentration. The slope of the linear fit represents the formation yield of 7-OH coumarin, or G-value, usually expressed in $mol.J^{-1}$. For concentrations below *ca* 20 µg/mL, G(7-OH coumarin) increases proportionally to the GNP concentration. This increase is then reduced and reaches a plateau for higher concentrations. This behavior, typically observed for radiolytic studies, testifies first for competition reactions i.e. hydroxyl radical scavenging by coumarin is in competition with other reactions such as $HO^{\bullet}$ recombination which is favored at high nanoparticle concentrations. It could also arise from GNP scavenging behavior as already evoked [27]. To convert G(7-OH coumarin) into $G(HO^{\bullet})$,

we extrapolated the formation yield of 7-OH coumarin to a concentration of 0 nM of GNPs (i.e., water alone) for which G-values are tabulated [28].

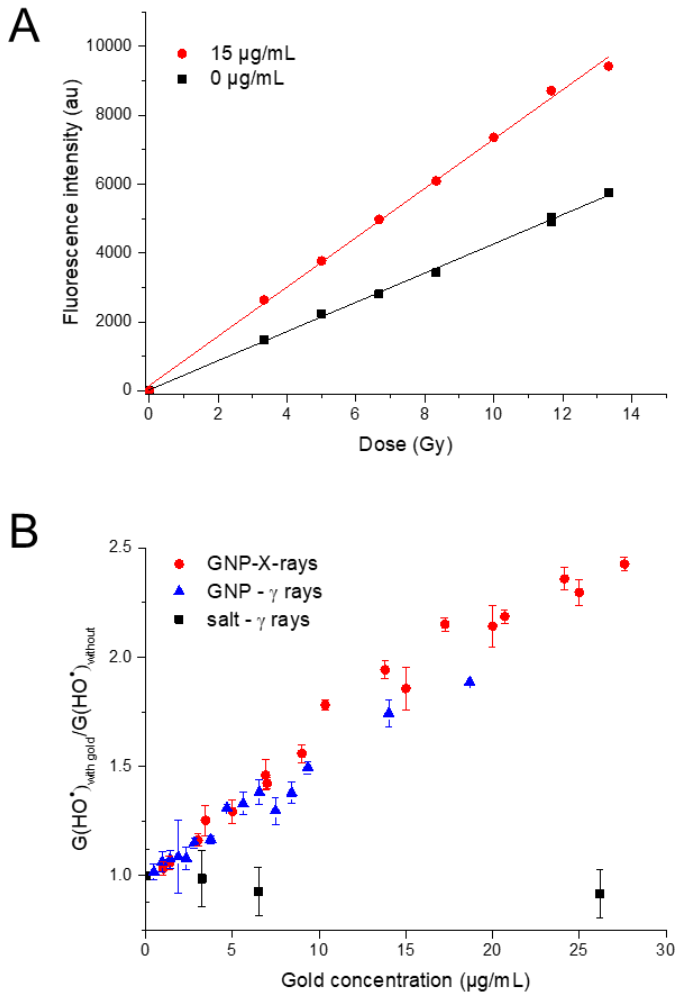

Figure 2 : Hydroxyl radical overproduction. A-Raw data obtained in a typical experiment. The fluorescence of 7-OH coumarin is plotted as a function of the irradiation dose. B- Comparison of hydroxyl radical yields between gold and water for different modalities. Red dots: 6 nm GNP irradiated with non monochromatic 17keV X-rays; Blue triangles: 6 nm GNP irradiated with γ-rays (1.2 MeV); Black squares: $KAuCl_4$ solution (salt) irradiated with γ-rays (1.2 MeV).

We plotted in Figure 2B the ratio of the G-values for hydroxyl radicals with and without gold, allowing an easier comparison with water radiolysis. We compared three conditions, i) when gold is irradiated as a salt ($KAuCl_4$), ii) when the same amount of gold is organized into a nanoparticle, iii) when the irradiation is performed with low (X-Rays) or high energy photons (γ-Rays). As expected, X-ray irradiation of 6 nm nanoparticles induces a significant radical

production increase as the efficiency to produce $HO^{\bullet}$ is doubled compared to water radiolysis for X-rays for 15 $\mu g.mL^{-1}$ GNP. As discussed below, tens of keV are expected to be the most efficient energy for gold enhancement considering only the difference in mass absorption of gold versus water (Figure 3). Nevertheless, under our conditions, the impact of the irradiation modality (X versus γ-rays) is negligible. Indeed, gamma rays (1.2 MeV) irradiation gives similar results which is unexpected from energy absorption prediction. Also, we compared the impact of nanoparticles with an equivalent amount of gold atoms ($KAuCl_4$). For this salt, G-values for $HO^{\bullet}$ are comparable to the one for water alone within the error bars as shown in Figure 2B. This clearly illustrates the fact that though equivalent numbers of gold atoms are present in the solution, nanoparticular organization is crucial for reactivity with ionizing radiations and radical production.

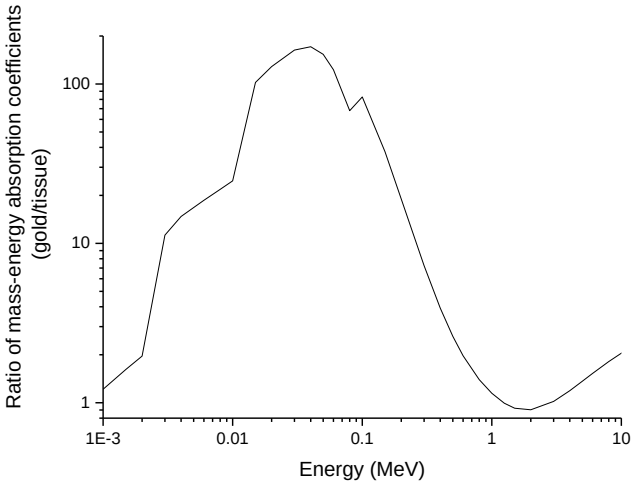

Figure 3: Ratio of the mass-energy absorption coefficients between gold and tissues (ref NIST)

In addition to hydroxyl radicals, the coumarin assay can be adapted to quantify solvated electrons by saturating the atmosphere with N_2O. As a N_2O-saturated solution corresponds to 25 mM of dissolved N_2O at 1 atm and 25°C [29] and given the rate constant of this reaction ($k= 9.10^9$ $L.mol^{-1}.s^{-1}$ [30]), the pseudo-one order kinetics leads to an electron capture in a few ns. Hydroxyl radicals are then produced and attack coumarin (Eq. 2). To extract the quantity of

electrons produced in the solution, we compared the 7-hydroxycoumarin detected under N_2O and N_2. Actually, oxygen was previously shown to impact the quantity of radical production [31], it is thus necessary to compare both systems with equivalent oxygen concentrations. Figure 4 represents the G-values for hydroxyl radicals for both atmospheres in the presence of GNP irradiated with X-rays. As for larger nanoparticles [31], the evolution of G($HO^{\bullet}$) as a function of the GNP concentration presents a linear increase for low concentrations (0-10 nM; 0- *ca* 15 µg/mL), and then reaches a plateau. Under N_2 atmosphere, up to three times more $HO^{\bullet}$ are quantified in the presence of 6 nm GNP. Under N_2O atmosphere, where 7-hydroxycoumarin fluorescence represents the contribution of $HO^{\bullet}$ and solvated electrons converted into $HO^{\bullet}$, a doubling of G($HO^{\bullet}$) compared to N_2 is observed whatever the GNP concentration. Thus for 6 nm GNP, as for 32 nm GNP [31], equivalent concentrations of hydroxyl radicals and solvated electrons are produced, corroborating the fact that nanoparticle irradiation induces additional radiolysis responsible for higher radical production.

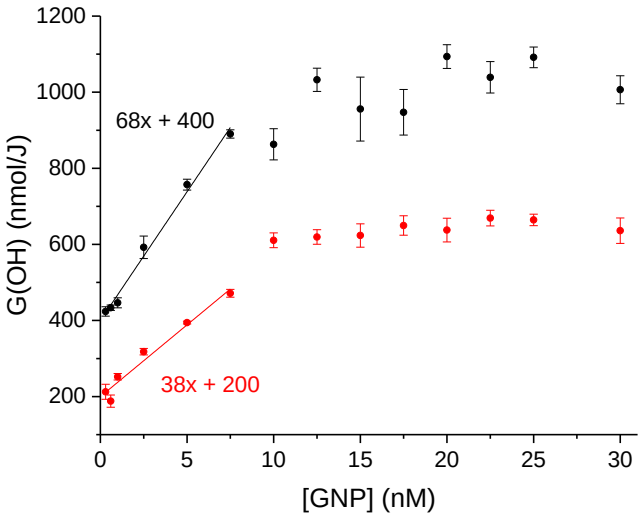

Figure 4: Hydroxy-coumarin quantification for GNP X-irradiated under different atmospheres.

In light of all these results, we can conclude that both hydroxyl radicals and electrons arise from specific properties of the solvent at the nanoparticle interface. Therefore, we proposed that a

specific water organization at the nanoparticle surface could be responsible for the high radical quantities produced. This hypothesis was tested for larger nanoparticles by adding a low concentration of NaCl as it could perturb this organization. The impact of salt was significant and induced a decrease in radical overproduction [31]. For smaller nanoparticles, another approach can be provided by simulation. We were interested in classical molecular dynamics which is known to be a useful tool for probing the structural organization of the first water solvation layer around the GNP [32]. Based on force fields, atomic-level simulation allows to vary the shape and size of the GNP, and to include ions, solvent molecules, and molecular ligands to represent the chemical environment. Here we illustrate the relevance of molecular dynamics simulations by comparing the solvation of a small nanoparticle, a cluster of 55 Au atoms (i.e. 1 nm in diameter), and a larger NP of 887 Au atoms (i.e. 3 nm in diameter). The size difference between the two GNPs will be considered sufficient to observe a size effect on the organization of the first solvation layer. All simulation conditions are similar to those used in [14]. Both GNPs were solvated in a water box using the rigid SPC/E model [33] to represent the water molecules. The GNP structure was considered as rigid to preserve the 3D organization. The water-gold interactions were considered using a dedicated force field [32]. In order to analyze the organization of the first water layer around the GNP, it is necessary to characterize its orientation relative to the surface. To do this, we have defined two angles, α and β, with respect to the GNP's center of mass. First, the angle α is defined by the dipole moment of the water molecule and the vector based on the center of mass and the oxygen atom. Second, β is defined as the angle between the normal of the water molecule and the vector between the GNP's center of mass and the oxygen atom. Three configurations of the orientation of a water molecule on the surface have been set up: (i) a flat configuration corresponds to α within 80° to 120° and β either below 30° or above 150°, (ii) an up configuration is defined for α less than or equal to 70° (whatever the value of β), (iii) a dangling configuration corresponds

to both α and β within 70° to 110°. Figure 5 shows the distribution of the α and β angles for which the colors highlight the configurations. The first observation is the high proportion of the up configurations during the simulation. These configurations correspond to interactions with the second solvation sphere by hydrogen bonds. As we change from the small to the large GNP, the flat/up ratio decreases from 0.86 to 0.62. This is the first sign of a reorganization of the hydrogen-bonding water network at the gold surface. Next, we observe a significant increase in the number of dangling bonds as the size of the GNP increases (from 7% to 17% with respect to the number of water molecules in the first shell). The analysis of such a local property on the GNP surface, combined with other macroscopic property calculations, led to the conclusion that GNPs used in the simulations of a size close to that of the experiments provide access to a surface large enough to induce a different organization of the water hydrogen bonding network [14].

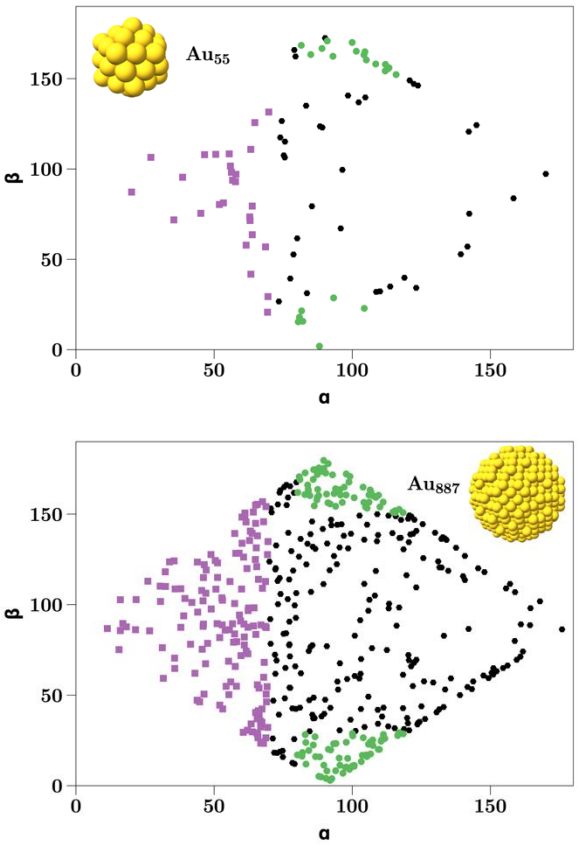

Figure 4: Distribution of α and β angles for Au_{55} (top) and Au_{887} (bottom). Up configurations in purple, flat configurations in green, and other configurations in black. As inserts, Au_{55} and Au_{887} GNPs are represented without the explicit representation of the solvent.

Discussion

One of the objectives of this work was to discuss the relation between energy absorption and the radical production in solution, when small GNPs were irradiated by low or high energy photons, with a special focus on hydroxyl radicals. Indeed, in radiobiology, a major role in driving indirect damage is attributed to hydroxyl radicals, which are considered the most powerful oxidant among the water radiolysis products. It should be noted that electrons with very low energy could also be responsible for direct cell component damages and they could play a role in NP radiosensitization as recently reviewed [34]. Real time, in-situ detection would

be the grail but given the short half-lives of such species and the huge absorption of gold colloidal solutions, this remains very challenging. Several techniques exist to quantify reactive oxygen species [35-36], but in this field, indirect detection of $HO^{\bullet}$ with EPR or fluorescent probes are the most common. One advantage is that the resulting products have a longer life time, allowing post-mortem analysis. Even when analyzing acellular NPs suspensions, attention should be paid to the specificity of the probe. For example 2,7-dichlorofluorescein diacetate (DCFDA) and its derivatives are unspecific to ROS or nitrogen species, dihydroethidium reacts with both hydroxyl and superoxide radicals. In addition, assays need to be optimized and NP-probe interferences need to be understood and taken into account [37] as they can quench both fluorescence and EPR signals.

Considering metallic nanoparticles as new therapeutic sensitizers, the first rationalization of their effect was dose enhancement. Dose enhancement by NP is based on their mass attenuation coefficient (μ/ρ) representing their energy absorption capacity. These values tabulated by the NIST indicate higher energy absorption by high-Z elements (Figure 3) and can allow us to calculate the quantitative enhancement prediction. For 6 nm diameter gold nanoparticles, there are about 6670 gold atoms per nanoparticle, assuming a particle density of 59 atoms.nm^{-3}. Taking the mass energy absorption coefficients for gold and water at 20 keV (65.22 cm^2.g^{-1} and 0.5503 cm^2.g^{-1} respectively), the extra X-ray energy absorption for a sample containing 20 µg/mL of these nanoparticles (equivalent to a mass fraction of 20.10^{-6}) is given by: 20.10^{-6} x 65.22 / 0.5503 = 2.10^{-3}. For bigger nanoparticles, the maximum expected is few percent, for example 2.5 % for 32 nm GNP [12]. Some proportion of this energy will then leave the nanoparticle in the form of photo- and Auger electrons, holes and lower energy photons. Some of the energy will be retained inside the nanoparticle as electrons loose energy by scattering from other atoms in the nanoparticle on their way. From Figure 2, it appears clearly that this higher energy absorption cannot account for the measured radical production as for a

concentration of 15 nM of GNP (20 µg/mL of gold), the quantity of radicals is multiplied by a factor 2, far from the 0.2 % calculated. This was also documented in other studies where 3 nm nanoparticles induce a radical quantity 2000 x higher than the absorption energy prediction [38] and Monte Carlo simulation of free radical production stated that $1mg.mL^{-1}$ of GNP should induce a dose deposition enhancement between 6 and 14% depending on their size and on the photon energy [39] confirming that high Z element energy absorption is not the only process responsible for radical overproduction. Also, comparing the gold and tissue or water mass energy absorption coefficients, it can be expected that no radical overproduction will be found for gamma rays. But, for 6 nm as for larger GNPs, noticeable equivalent hydroxyl radical and solvated electrons overproduction was measured. In addition, we compared GNP radical production with gold salt ($KAuCl_4$) for equivalent gold concentration. From Figure 2, we can conclude that there is a huge effect of the nanoparticle structure as we were not able to evidence any radical overproduction for gold salt though we measured a huge increase for equivalent gold atoms organized in a nanoparticle. Thus, the regular arguments still evoked in the present literature have to be tackled cautiously.

As physical dose increase could only contribute weakly to radical production, other mechanisms must be considered. This is especially true when considering other radiosensitizing NPs such as nanodiamonds [40-41], for which no difference in absorption coefficients exist, or NPs of many lower atomic number element oxides [42]. Different hypotheses are proposed in the litterature, which are not mutually exclusive or universal. NPs could act as electron or hole donor as described in semiconductors in photocatalysis [35]. Some NPs could present catalytic surfaces or dissolution of ions, allowing Haber-Weiss and Fenton reactions [43]. It has to be noted that for some systems, NPs reactivity occurs without irradiation. For example V_2O_5 NPs generate *per se* 1.5 µM of hydroxyl radicals and an additional 1.8 µM after 10 Gy [42]. It was

also proposed that some NPs could act as an electron relay, facilitating the transfer between electron donors and acceptors independently of irradiation [44], or could lower the ionizing potential of surrounding water molecules. We propose that this could be achieved through a different organization of water molecules in the vicinity of the NP surface, as investigated in this paper, that could impact their structural and electronic properties [14]. This hypothesis was challenged for larger nanoparticles by the addition of a low quantity of NaCl that should disturb water organization at the nanoparticle surface. Salt concentration being correlated with a decrease of hydroxyl radical, we consider that interfacial water plays a crucial role in radical production.

Conclusion

A first progress to decipher the mechanism of radical production by irradiated nanoparticles was to focus on the physico-chemical step i.e. reactive species quantification. In this study, we showed that gold atoms become efficient to generate radicals only when they are organized as nanoparticles. Coupling experimental data with simulation approach, we were able to evidence that water network at the nanoparticle surface has a specific organization that could be responsible for high quantity radical production.

Acknowledgements

The authors thank James Beauvil for gamma irradiations.

The present work has benefited from Imagerie-Gif core facility supported by l'Agence Nationale de la Recherche (ANR-11-EQPX-0029/Morphoscope, ANR-10-INBS-04/FranceBioImaging ; ANR-11-IDEX-0003-02/ Saclay Plant Sciences).

References

[1]. Oliveira, B. B.; Ferreira, D.; Fernandes, A. R.; Baptista, P. V., Engineering gold nanoparticles for molecular diagnostics and biosensing. *Wiley Interdisciplinary Reviews-Nanomedicine and Nanobiotechnology* **2023,** *15* (1), 28.
[2]. Kesharwani, P.; Ma, R. Y.; Sang, L.; Fatima, M.; Sheikh, A.; Abourehab, M. A. S.; Gupta, N.; Chen, Z. S.; Zhou, Y., Gold nanoparticles and gold nanorods in the landscape of cancer therapy. *Molecular Cancer* **2023,** *22* (1), 31.
[3]. Dreaden, E. C.; Alkilany, A. M.; Huang, X.; Murphy, C. J.; El-Sayed, M. A., The golden age: gold nanoparticles for biomedicine. *Chemical Society Reviews* **2012,** *41* (7), 2740-2779.
[4]. Hainfeld, J. F.; Slatkin, D. N.; Focella, T. M.; Smilowitz, H. M., Gold nanoparticles: a new X-ray contrast agent. *Br J Radiol* **2006,** *79* (939), 248-53.
[5]. Brun, E.; Sicard-Roselli, C., Actual questions raised by nanoparticle radiosensitization. *Radiation Physics and Chemistry* **2016,** *128*, 134-142.
[6]. Kempson, I., Mechanisms of nanoparticle radiosensitization. *Wiley Interdisciplinary Reviews-Nanomedicine and Nanobiotechnology* **2021,** *13* (1).
[7]. Penninckx, S.; Heuskin, A. C.; Michiels, C.; Lucas, S., Gold Nanoparticles as a Potent Radiosensitizer: A Transdisciplinary Approach from Physics to Patient. *Cancers* **2020,** *12* (8).
[8]. Incerti, S.; Suerfu, B.; Xu, J.; Ivantchenko, V.; Mantero, A.; Brown, J. M. C.; Bernal, M. A.; Francis, Z.; Karamitros, M.; Tran, H. N., Simulation of Auger electron emission from nanometer-size gold targets using the Geant4 Monte Carlo simulation toolkit. *Nucl Instrum Meth B* **2016,** *372*, 91-101.
[9]. Poignant, F.; Monini, C.; Testa, E.; Beuve, M., Influence of gold nanoparticles embedded in water on nanodosimetry for keV photon irradiation. *Med Phys* **2021,** *48* (4), 1874-1883.
[10]. Rudek, B.; McNamara, A.; Ramos-Mendez, J.; Byrne, H.; Kuncic, Z.; Schuemann, J., Radio-enhancement by gold nanoparticles and their impact on water radiolysis for x-ray, proton and carbon-ion beams. *Physics in Medicine and Biology* **2019,** *64* (17).
[11]. Rosa, S.; Connolly, C.; Schettino, G.; Butterworth, K. T.; Prise, K. M., Biological mechanisms of gold nanoparticle radiosensitization. *Cancer Nanotechnol* **2017,** *8* (1), 2.
[12]. Sicard-Roselli, C.; Brun, E.; Gilles, M.; Baldacchino, G.; Kelsey, C.; McQuaid, H.; Polin, C.; Wardlow, N.; Currell, F., A New Mechanism for Hydroxyl Radical Production in Irradiated Nanoparticle Solutions. *Small* **2014,** *10* (16), 3338-3346.
[13]. Spinks, J. W. T.; Woods, R. J., *Introduction to radiation chemistry*. third ed.; Wiley: New-York, 1990.
[14]. Tandiana, R.; Brun, E.; Sicard-Roselli, C.; Domin, D.; Van-Oanh, N. T.; Clavaguera, C., Probing the structural properties of the water solvation shell around gold nanoparticles: A computational study. *Journal of Chemical Physics* **2021,** *154* (4).
[15]. Hainfeld, J. F.; Slatkin, D. N.; Smilowitz, H. M., The use of gold nanoparticles to enhance radiotherapy in mice. *Physics in Medicine and Biology* **2004,** *49* (18), N309-15.
[16]. Kaura, H.; Pujaria, G.; Semwalb, M. K.; Sarmaa, A.; Kumar Avasthi, D., In vitro studies on radiosensitization effect of glucose capped gold nanoparticles in photon and ion irradiation of HeLa cell. . *Nuclear Instruments and Methods in Physics Research Section B: Beam Interactions with Materials and Atoms.* **2013,** *301*, 7-11.
[17]. Brun, E.; Sanche, L.; Sicard-Roselli, C., Parameters governing gold nanoparticle X-ray radiosensitization of DNA in solution. *Colloids and Surfaces B: Biointerfaces* **2009,** *72* (1), 128-34.
[18]. Li, W. B.; Belchior, A.; Beuve, M.; Chen, Y. Z.; Di Maria, S.; Friedland, W.; Gervais, B.; Heide, B.; Hocine, N.; Ipatov, A.; Klapproth, A. P.; Li, C. Y.; Li, J. L.; Multhoff, G.; Poignant, F.; Qiu, R.; Rabus, H.; Rudek, B.; Schuemann, J.; Stangl, S.; Testa, E.; Villagrasa, C.; Xie, W. Z.; Zhang, Y. B., Intercomparison of dose enhancement ratio and secondary electron spectra for gold nanoparticles irradiated by X-rays calculated using multiple Monte Carlo simulation codes. *Phys Med* **2020,** *69*, 147-163.
[19]. Velten, C.; Tome, W. A., Reproducibility study of Monte Carlo simulations for nanoparticle dose enhancement and biological modeling of cell survival curves. *Biomedical Physics & Engineering Express* **2023,** *9* (4), 11.
[20]. Fan, M.; Han, Y.; Gao, S. T.; Yan, H. Y.; Cao, L. Z.; Li, Z. H.; Liang, X. J.; Zhang, J. C., Ultrasmall gold nanoparticles in cancer diagnosis and therapy. *Theranostics* **2020,** *10* (11), 4944-4957.

[21]. Balfourier, A.; Luciani, N.; Wang, G.; Lelong, G.; Ersen, O.; Khelfa, A.; Alloyeau, D.; Gazeau, F.; Carn, F., Unexpected intracellular biodegradation and recrystallization of gold nanoparticles. *Proceedings of the National Academy of Sciences of the United States of America* **2020,** *117* (1), 103-113.
[22]. Huang, K. Y.; Ma, H. L.; Liu, J.; Huo, S. D.; Kumar, A.; Wei, T.; Zhang, X.; Jin, S. B.; Gan, Y. L.; Wang, P. C.; He, S. T.; Zhang, X. N.; Liang, X. J., Size-Dependent Localization and Penetration of Ultrasmall Gold Nanoparticles in Cancer Cells, Multicellular Spheroids, and Tumors in Vivo. *Acs Nano* **2012,** *6* (5), 4483-4493.
[23]. Gilles, M.; Brun, E.; Sicard-Roselli, C., Gold nanoparticles functionalization notably decreases radiosensitization through hydroxyl radical production under ionizing radiation. *Colloids and Surfaces B: Biointerfaces* **2014,** *123*, 770-777.
[24]. Grellet, S.; Tzelepi, K.; Roskamp, M.; Williams, P.; Sharif, A.; Slade-Carter, R.; Goldie, P.; Whilde, N.; Smialek, M. A.; Mason, N. J.; Golding, J. P., Cancer-selective, single agent chemoradiosensitising gold nanoparticles. *Plos One* **2017,** *12* (7), 21.
[25]. Mai, T.; Hilt, J. Z., Functionalization of iron oxide nanoparticles with small molecules and the impact on reactive oxygen species generation for potential cancer therapy. *Colloids and Surfaces a-Physicochemical and Engineering Aspects* **2019,** *576*, 9-14.
[26]. Louit, G.; Foley, S.; Cabillic, J.; Coffigny, H.; Taran, F.; Valleix, A.; Renault, J. P.; Pin, S., The reaction of coumarin with the OH radical revisited: hydroxylation product analysis determined by fluorescence and chromatography. *Radiation Physics and Chemistry* **2005,** *72* (2–3), 119-124.
[27]. Ionita, P.; Spafiu, F.; Ghica, C., Dual behavior of gold nanoparticles, as generators and scavengers for free radicals. *J Mater Sci* **2008,** *43* (19), 6571-6574.
[28]. Fulford, J.; Nikjoo, H.; Goodhead, D. T.; O'Neill, P., Yields of SSB and DSB induced in DNA by Al(K) ultrasoft X-rays and alpha-particles: comparison of experimental and simulated yields. *International Journal of Radiation Biology* **2001,** *77* (10), 1053-66.
[29]. Spinks, J. W. T.; Woods, R. J., *An Introduction to Radiation Chemistry; 3rd ed.; Wiley-Interscience publication: New York, USA.* 1990.
[30]. Buxton, G. V.; Greenstock, C. L.; Helman, W. P.; Ross, A. B., Critical-Review of Rate Constants for Reactions of Hydrated Electrons, Hydrogen-Atoms and Hydroxyl Radicals in Aqueous-Solution. *Journal of Physical Chemical Reference Data* **1988,** *17* (2), 513-886.
[31]. Gilles, M.; Brun, E.; Sicard-Roselli, C., Quantification of hydroxyl radicals and solvated electrons produced by irradiated gold nanoparticles suggests a crucial role of interfacial water. *Journal of Colloid and Interface Science* **2018,** *525*, 31-38.
[32]. Berg, A.; Peter, C.; Johnston, K., Evaluation and Optimization of Interface Force Fields for Water on Gold Surfaces. *Journal of Chemical Theory and Computation* **2017,** *13* (11), 5610-5623.
[33]. Chatterjee, S.; Debenedetti, P. G.; Stillinger, F. H.; Lynden-Bell, R. M., A computational investigation of thermodynamics, structure, dynamics and solvation behavior in modified water models. *The Journal of Chemical Physics* **2008,** *128* (12).
[34]. Zheng, Y.; Sanche, L., Mechanisms of Nanoscale Radiation Enhancement by Metal Nanoparticles: Role of Low Energy Electrons. *International Journal of Molecular Sciences* **2023,** *24* (5).
[35]. Nosaka, Y.; Nosaka, A. Y., Generation and Detection of Reactive Oxygen Species in Photocatalysis. *Chemical Reviews* **2017,** *117* (17), 11302-11336.
[36]. Zhang, Y. F.; Dai, M. H.; Yuan, Z. H., Methods for the detection of reactive oxygen species. *Analytical Methods* **2018,** *10* (38), 4625-4638.
[37]. Tournebize, J.; Sapin-Minet, A.; Schneider, R.; Boudier, A.; Maincent, P.; Leroy, P., Simple spectrophotocolorimetric method for quantitative determination of gold in nanoparticles. *Talanta* **2011,** *83* (5), 1780-1783.
[38]. Cheng, N. N.; Starkewolf, Z.; Davidson, R. A.; Sharmah, A.; Lee, C.; Lien, J.; Guo, T., Chemical enhancement by nanomaterials under X-ray irradiation. *Journal of the American Chemical Society* **2012,** *134* (4), 1950-3.

[39]. Poignant, F.; Charfi, H.; Chan, C. H.; Dumont, E.; Loffreda, D.; Testa, E.; Gervais, B.; Beuve, M., Monte Carlo simulation of free radical production under keV photon irradiation of gold nanoparticle aqueous solution. Part I: Global primary chemical boost. *Radiation Physics and Chemistry* **2020,** *172*.
[40]. Brun, E.; Girard, H. A.; Arnault, J. C.; Mermoux, M.; Sicard-Roselli, C., Hydrogen plasma treated nanodiamonds lead to an overproduction of hydroxyl radicals and solvated electrons in solution under ionizing radiation. *Carbon* **2020,** *162*, 510-518.
[41]. Kurzyp, M.; Girard, H. A.; Cheref, Y.; Brun, E.; Sicard-Roselli, C.; Saada, S.; Arnault, J. C., Hydroxyl radical production induced by plasma hydrogenated nanodiamonds under X-ray irradiation. *Chem Commun* **2017,** *53* (7), 1237-1240.
[42]. Guerreiro, A.; Chatterton, N.; Crabb, E. M.; Golding, J. P., A comparison of the radiosensitisation ability of 22 different element metal oxide nanoparticles using clinical megavoltage X-rays. *Cancer Nanotechnology* **2019,** *10* (1), 20.
[43]. Kessler, A.; Hedberg, J.; Blomberg, E.; Odnevall, I., Reactive Oxygen Species Formed by Metal and Metal Oxide Nanoparticles in Physiological Media-A Review of Reactions of Importance to Nanotoxicity and Proposal for Categorization. *Nanomaterials* **2022,** *12* (11).
[44]. Shcherbakov, V.; Denisov, S. A.; Mostafavi, M., A mechanistic study of gold nanoparticles catalysis of O-2 reduction by ascorbate and hydroethidine, investigating reactive oxygen species reactivity. *Rsc Advances* **2023,** *13* (13), 8557-8563.